J Therm Anal Calorim (2010) 100:183–189
DOI 10.1007/s10973-009-0444-2

The stability of inclusion compounds under heating

Part 2. Inclusion compounds of layered zinc camphorate, linked by linear N-donor ligands

V. Logvinenko · D. Dybtsev · V. Fedin · V. Drebushchak · M. Yutkin

Received: 31 July 2009 / Accepted: 25 August 2009 / Published online: 9 October 2009

Abstract The thermal decomposition of three inclusion compounds: $[Zn_2(camph)_2dabco]\cdot DMF\cdot H_2O$, $[Zn_2(camph)_2bipy]\cdot 3DMF\cdot H_2O$ and $[Zn_2(camph)_2bpe]\cdot 5DMF\cdot H_2O$ was studied in the inert atmosphere. TG and DTG curves confirm multi-step decomposition process, the dehydration being the first step. Thermogravimetric data (obtained at different rates of linear heating) were processed with computer program (with 'Model-free' approach). Kinetic parameters of decomposition were calculated for the DMF multi-step removal, the processes are described by Avrami–Erofeev equations. The connection between the kinetic parameters and structural features of the host frameworks (ligand linker lengths and porous-free volumes) are discussed.

Keywords Coordination compounds · Inclusion compounds · 'Model-free' kinetics · Non-isothermal kinetics

Introduction

Coordination polymers with porous structure can form inclusion compounds, and hence successfully used for gas storage and selective separation [1]. The important subclass of these materials is homochiral porous coordination polymers, which contain regular asymmetric centers incorporated into the metal–organic framework. They are believed to be the best suited for stereoselective sorption and chiral resolution of racemate mixtures onto different enantiomeres. The quantitative information about thermal (kinetic) stability of such compounds is important for the understanding of "composition–structure–properties" regularities; however, such measurements have never been performed so far.

V. Logvinenko (✉) · D. Dybtsev · V. Fedin · V. Drebushchak · M. Yutkin
Nikolaev Institute of Inorganic Chemistry, Siberian Branch of Russian Academy of Sciences, Ac. Lavrentyev Ave. 3, 630090 Novosibirsk-90, Russia
e-mail: val@che.nsk.su

Experimental

Synthesis of inclusion compounds

All inclusion compounds were synthesized by the interaction between zinc nitrate, camphoric acid and a linear N-donor ligand linker (in ratio 2:2:1) in DMF solution; the composition of obtained crystals: $[Zn_2(camph)_2dabco]\cdot DMF\cdot H_2O$, $[Zn_2(camph)_2bipy]\cdot 3DMF\cdot H_2O$ and $[Zn_2(camph)_2bpe]\cdot 5DMF\cdot H_2O$ ($H_2camph = C_8H_{14}(COOH)_2$, $dabco = C_6H_{12}N_2$, $bipy = C_{10}H_8N_2$, $bpe = C_{12}H_{10}N_2$, $DMF = C_3H_7NO$). Method of elemental (C, H, N) analysis was used for the determination of the composition of the crystals; the solvent weight loss corresponds to the indicated quantities of DMF + H_2O [2]. The linker ligand length increases in the series: 4.5 (dabco), 8.0 (bipy) and 10.5 Å (bpe), corresponding free profiles of intersecting channels are 3 × 3.5, 5 × 7 and 5 × 10 Å, and free accessible volumes in the porous frameworks increase similarly 31, 49 and 55% [2].

Thermal analysis

TG measurements were carried out on a Netzsch thermal analyzer TG 209 F1. The experiments were performed in argon flow (35 cm^3 min^{-1}), at heating rates of 5, 10 and 20 K min^{-1}, the sample mass was kept cca 12.0–15.0 mg. Thermomechanical analysis (dilatometry) was carried out

on a Netzsch thermal analyzer TMA 202; the powder layer thickness was 1.02–1.03 mm (with sample mass 42–45 mg).

Kinetic analysis under non-isothermal conditions

Thermogravimetric data were processed with the computer program Netzsch Thermokinetics 2 (Version 2004.05). Special program module 'Model-free', based on the well-known works [3–9], allows processing several thermogravimetric curves, obtained with different heating rates, and calculating energy of activation, without the preliminary information about the kinetic topochemical equations.

The program 'Ozawa–Flynn–Wall analysis' was used for the calculation of activation energies for the every experimental point of fractional conversion (in the interval $0.005 < \alpha < 0.995$). 'Ozawa–Flynn–Wall analysis' is based on the dependence between the heating rate and inverse temperature. We used further the same set of experimental data for searching the topochemical equation (the selection was done from 16 equations: chemical reaction on the interface, nucleation and diffusion). This calculation is made by the improved differential method of Borchardt–Daniels, with multiple linear regression method. It is very important that the interval of conversion degree (α) for this calculation can be chosen on the base of the relative constancy of the calculated kinetic parameters from 'Ozawa–Flynn–Wall Analysis'. The F test is used for the search of the best kinetic description (see tables).

The F test is used for the statistical control of the obtained equation. It tests the residual variances of the individual models against one another and answer the question, whether the models differ significantly (statistically speaking). If $F_{exp(1)} \approx F_{exp(2)}$ for two equations, there is no reason to assume that the first model is better for the characterization of the experiment. The statistical quantile, F_{crit}, is obtained for a level of significance, 0.05.

If the calculation results in two or three kinetic equations with near values of the correlation coefficients and the F test, but with noticeably different values of kinetics parameters, it is more correct to choose the equation with activation energy values near to the data of 'Model free' module program.

The discrimination of two steps was very relative in this search of topochemical equations (Tables 1, 2, 3), but it helps to find the most reliable ones.

The special program of nonlinear regression is useful in search of the full set of kinetic parameters for multi-step processes. The closest fit between activation energies from "Model-free" analysis and the data from nonlinear regression calculation is important from a physical–chemical point of view; so the authors of used computer program recommend to fix E_a values (obtained by linear regression, and congruent with E_a, from "Model-free" analysis) during calculations with this program.

The random error in activation energy values for such reversible decomposition reaction under such experiments usually is about 10%, and we took this into consideration.

The computer program "NETZSCH Thermokinetics 2" gives the possibility to estimate the steps contribution (in Δm percentage) after this nonlinear regression calculation.

Table 1 Data of linear regression for decomposition of $[Zn_2(camph)_2dabco]\cdot DMF$

10.0–50.0% of conversion degree				50.0–95.0% of conversion degree			
F_{exp}	F_{crit}	f_{active}	Equation	F_{exp}	F_{crit}	f_{active}	Equation
1.00	1.68	42	An: $E = 76.7 \pm 3.7$ kJ mol^{-1}	1.00	1.42	91	Fn: $E = 71.2 \pm 3.6$ kJ mol^{-1}
2.68	1.68	42	Fn	10.92	1.42	91	An
2.74	1.68	41	CnB	61.74	1.42	92	D3
2.75	1.67	43	D3	150.39	1.42	91	C1B
2.76	1.68	41	Bna	595.59	1.42	92	B1

Table 2 Data of linear regression for decomposition of $[Zn_2(camph)_2bipy]\cdot 3DMF\cdot H_2O$

05.0–40.0% of conversion degree				40.0–95.0% of conversion degree			
F_{exp}	F_{crit}	f_{active}	Equation	F_{exp}	1.70	f_{active}	Equation
1.00	1.69	41	An: $E = 125 \pm 10$ kJ mol^{-1}	1.00	1.70	40	D3: $E = 89.8 \pm 1.5$ kJ mol^{-1}
3.41	1.68	42	D3: $E = 91.8 \pm 4.6$ kJ mol^{-1}	1.06	1.70	39	An: $E = 99.1 \pm 3.7$ kJ mol^{-1}
5.14	1.69	41	Fn	11.07	1.70	39	Fn
5.27	1.69	40	Cn B	11.36	1.71	38	CnB
5.86	1.69	40	Bna	369.19	1.71	38	Bna

Table 3 Data of linear regression for decomposition of $[Zn_2(camph)_2bpe]\cdot 5DMF$

05.0–40.0% of conversion degree				40.0–95.0% of conversion degree			
F_{exp}	F_{exp}	F_{exp}	Equation	F_{exp}	F_{crit}	f_{active}	Equation
1.00	1.00	52	An: $E = 28.1 \pm 1.9$ kJ mol^{-1}	1.00	1.62	48	An: $E = 47.7 \pm 0.1$ kJ mol^{-1}
1.29	1.29	52	Fn	1.38	1.62	48	Fn
1.32	1.32	51	Cn B	1.41	1.62	47	Cn B
1.32	1.32	51	Bna	1.41	1.62	47	Bna
4.67	4.67	53	D3	15.65	1.61	49	D3

Results and discussion

All compounds lose both water and dimethylformamide molecules under heating, next farther step of decomposition is the N-donor ligand (linker) loss (>330 °C for dabco and >240 °C for bipy and bpe). The mass loss is multi-step process, which was confirmed by DTG curves, and we attribute the very first small (and strongly pronounced by DTG) step of mass loss to the water removal (cca 2.0 and 1.7% mass loss for bipy and bpe derivations), while the water molecule having time to move away from dabco derivation under the action of argon flow still before switching on the heating. The decomposition of $[Zn_2(camph)_2bpe]\cdot 5DMF\cdot H_2O$ is the typical example (Fig. 1).

As a result, we cut off cca 1.7–2.0% of mass loss from the beginning of TG curves for $[Zn_2(camph)_2bipy]\cdot 3DMF\cdot H_2O$ and $[Zn_2(camph)_2bpe]\cdot 5DMF\cdot H_2O$; the residuary mass loss was about 10.0, 23.8 and 33.5% for dabco, bipy, bpe compounds, respectively. These refined TG curves (Fig. 2 as example) are processed by computer program, although such curves' pre-treating is imperfect and incomplete, curves onsets are distorted.

$$[Zn_2(camph)_2dabco]\ DMF \rightarrow [Zn_2(camph)_2dabco] + DMF\ \uparrow$$

"Model-free" data are represented on Fig. 3.

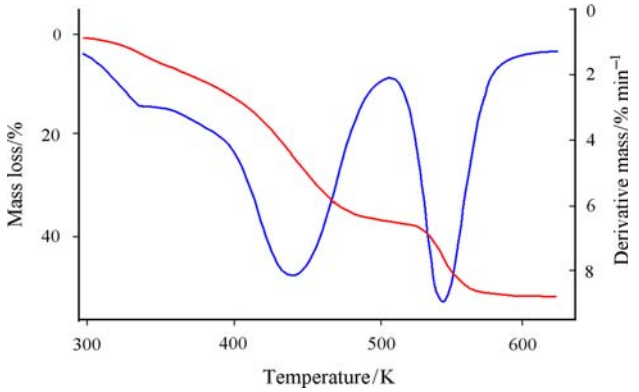

Fig. 1 TG and DTG curves for $[Zn_2(camph)_2bpe]\cdot 5DMF\cdot H_2O$ decomposition, $m \approx 12.0$ mg, heating rate 20 K min^{-1}, argon flow 35 cm^3 min^{-1}

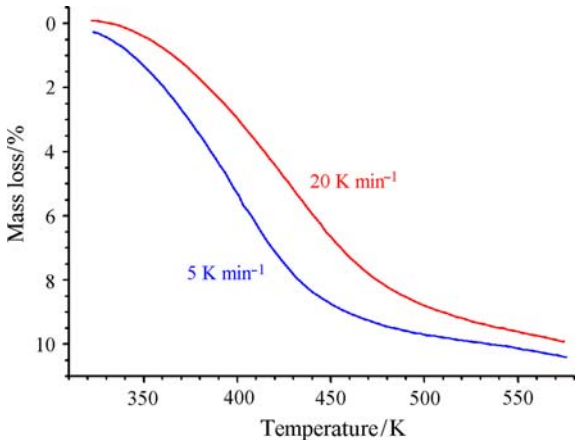

Fig. 2 TG curves for $[Zn_2(camph)_2dabco]\cdot DMF$ decomposition, $m \approx 12.0$ mg, heating rate 5 and 20 K min^{-1}, argon flow 35 cm^3 min^{-1}

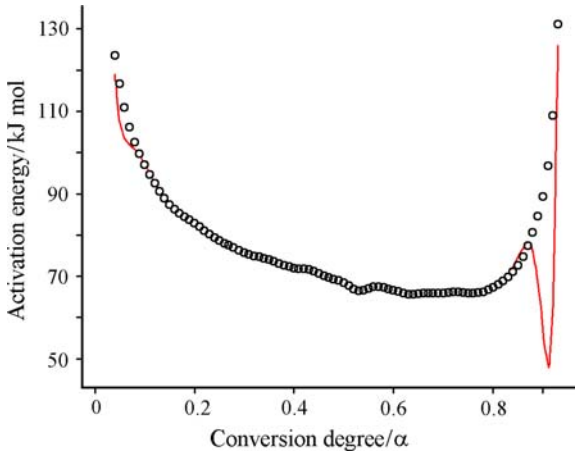

Fig. 3 Ozawa–Flynn–Wall analysis for $[Zn_2(camph)_2dabco]\cdot DMF$ decomposition: activation energies depending on the conversion degree

The beginning of the decomposition ($\alpha < 50\%$) is distorted by water elimination, the activation energy is constant for $50\% < \alpha < 85\%$; we considered the second step of decomposition as the process of guest molecules elimination.

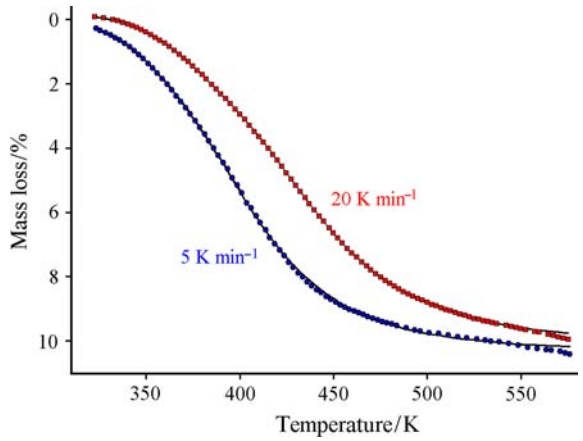

Fig. 4 $[Zn_2(camph)_2dabco]\cdot DMF$ decomposition. Data processing: curves fitting of non-linear regression, simulated with An (the first step) and Fn (the second step) equations. The region of conversion degree for calculation: $0.01 \leq \alpha \leq 0.99$. Experimental points, calculated lines

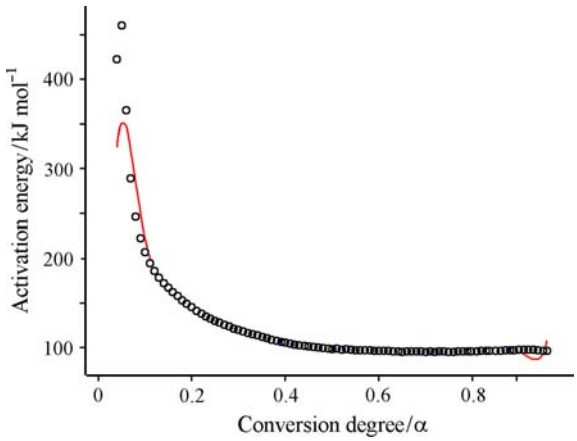

Fig. 5 Ozawa–Flynn–Wall analysis for $[Zn_2(camph)_2bipy]\cdot 3DMF$ decomposition: activation energies depending on the conversion degree

Nonlinear regression (Fig. 4)

Energy of activation E_1 (76.7 kJ mol^{-1}) was fixed before the first part of calculation. Data of nonlinear regression ($\alpha = 0.01$–0.99):

The first step, An, $f_1(\alpha) = (1 - \alpha)\ [-\ln(1 - \alpha)]^{0.77}$, $E_1 = 76.7$ kJ mol^{-1}, lg A $= 8.9 \pm 0.1$.
The second step, Fn, $f_2(\alpha) = (1 - \alpha)^{2.7}$, $E_1 = 64 \pm 2$ kJ mol^{-1}, lg A $= 5.8 \pm 0.2$.

We cancel the fixing of E_1, the new variant of calculation gives results:

The first step, An, $f_1(\alpha) = (1 - \alpha)\ [-\ln(1 - \alpha)]^{0.72}$, $E_1 = 89 \pm 4$ kJ mol^{-1}, lg A $= 10.9 \pm 0.7$.
The second step, Fn, $f_2(\alpha) = (1 - \alpha)^{2.7}$, $E_1 = 63 \pm 1$ kJ mol^{-1}, lg A $= 5.7 \pm 0.2$.

These data are consistent with Ozawa analysis (Fig. 3: $E_1 > E_2$). Correlation coefficient is 0.9999. We estimated the steps contribution: the first step is 21.7% and the second step is 78.3% of the decomposition; it refined the primary data of Ozawa model.

$$\left[Zn_2(camph)_2bipy\right]\ 3DMF \rightarrow \left[Zn_2(camph)_2bipy\right] + 3DMF\uparrow$$

"Model-free" data are represented on Fig. 5. The beginning of the decomposition ($\alpha < 40\%$) is distorted by water elimination, the activation energy is constant for $40\% < \alpha < 95\%$; we considered the second step of decomposition as the process of guest molecules elimination.

Equations D3 and An in the second step are indistinguishable by F test. Two variants of the linear regression for full curve ($\alpha = 0.005$–0.999) processing:

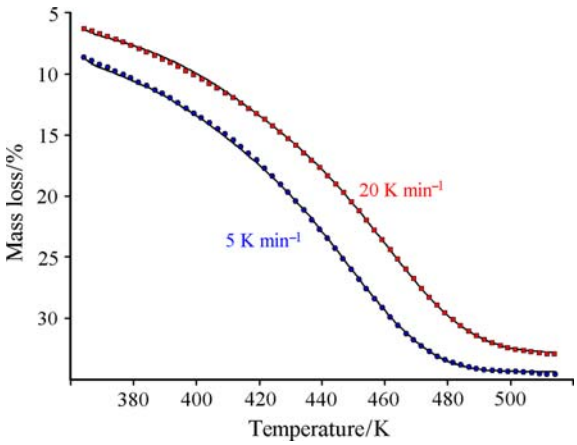

Fig. 6 $[Zn_2(camph)_2bipy]\cdot 3DMF$ decomposition. Data processing: curves fitting of non-linear regression, simulated with An (the first step) and An (the second step) equations. The region of conversion degree for calculation: $0.001 \leq \alpha \leq 0.999$. Experimental points, calculated lines

(1) An, $f(\alpha) = (1 - \alpha)\ [-\ln(1 - \alpha)]^{0.49}$, $E = 105 \pm 3$ kJ mol^{-1}, lg A $= 10.3 \pm 0.4$. Correlation coefficient is 0.9995.
(2) D3, $f(\alpha) = (1 - \alpha)^{1/3}/[(1 - \alpha)^{-1/3} - 1]$, $E = 88.1 \pm 1.5$ kJ mol^{-1}, lg A $= 7.2 \pm 0.2$.

Correlation coefficient is 0.9996. Obtained $E = 88.1$ mol^{-1} is too small (Fig. 5), and we used An equations for nonlinear regression calculations:

Nonlinear regression (Fig. 6)

The first step, An, $f_1(\alpha) = (1 - \alpha)\ [-\ln(1 - \alpha)]^{0.46}$, $E_1 = 145 \pm 1$ kJ mol^{-1}, lg A $= 17.5 \pm 0.1$.

The second step, An, $f_2(\alpha) = (1 - \alpha)\ [-\ln(1 - \alpha)]^{0.71}$, $E_2 = 95 \pm 4$ kJ mol^{-1}, lg A = 9.0 ± 0.4.

These data are consistent with Ozawa analysis (Fig. 5: $E_1 > E_2$). Correlation coefficient is 0.99994. The first step is 19.1% and the second step is 80.9% of the decomposition; it refined the primary data of Ozawa model.

$$\left[Zn_2(camph)_2bpe\right] 5DMF \rightarrow \left[Zn_2(camph)_2bpe\right] + 5DMF\uparrow$$

"Model-free" data are represented on Fig. 7. The very beginning of the decomposition ($\alpha < 05\%$) is distorted by water elimination, the activation energy variability can be connected with two-step process ($5\% < \alpha < 95\%$); we considered this part of decomposition as the process of guest molecules elimination.

Nonlinear regression (Fig. 8)

Energies of activation E_1 (28.1 kJ mol^{-1}) and E_2 (47.7 kJ mol^{-1}) were fixed before the calculation. Data of nonlinear regression ($\alpha = 0.01$–0.95):

The first step, An, $f_1(\alpha) = (1 - \alpha)\ [-\ln(1 - \alpha)]^{0.74}$, $E_1 = 28.1$ kJ mol^{-1}, lg A = 0.8 ± 0.1.
The second step, An, $f_2(\alpha) = (1 - \alpha)\ [-\ln(1 - \alpha)]^{1.52}$, $E_2 = 47.7$ kJ mol^{-1}, lg A = 4.6 ± 0.2.

These data are consistent with Ozawa analysis (Fig. 7: $E_1 < E_2$). Correlation coefficient is 0.9999. The first step is 27.2% and the second step is 72.8% of the decomposition; it refined the primary data of Ozawa model.

These three inclusion compounds have primitive cubic topology and could be considered isotypical. However, they have different packing mode of $[Zn_2(camph)_2]$-layers because of different linear N-donor ligands: dabco-compound has these layers exactly atop of each other, alternating

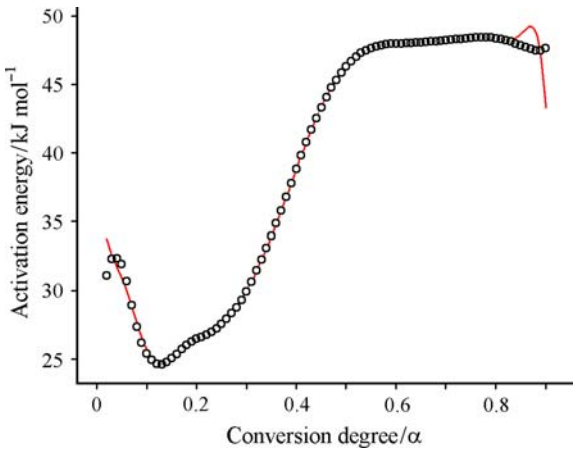

Fig. 7 Ozawa–Flynn–Wall analysis for $Zn_2(camph)_2bpe]\cdot5DMF$ decomposition: activation energies depending on the conversion degree

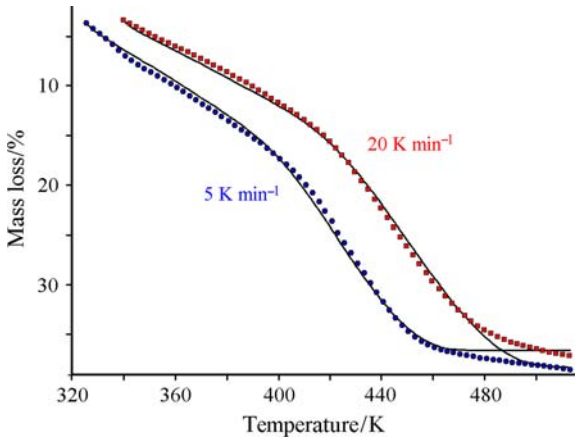

Fig. 8 $Zn_2(camph)_2bpe]\cdot5DMF$ decomposition. Data processing: curves fitting of non-linear regression, simulated with An (the first step) and An (the second step) equations. The region of conversion degree for calculation: $0.01 \leq \alpha \leq 0.95$. Experimental points, calculated lines

layout in bipy-compound, while the packing mode of these layers is irregular in bpe-compound [2].

The structure of the dabco-contained inclusion compound is rather rigid and stable because of the link shortness, the "empty" matrix structure (31% of the emptiness after decomposition) is fully stable; this results in middle value of activation energy: for the elastic deformation (without destruction) of the matrix structure during DMF release. The sample volume change corresponds to this data: $[Zn_2(camph)_2dabco]\cdot DMF\cdot H_2O$ does not change the volume practically (Fig. 9, curve 2). These properties are more or less similar to inclusion compounds ($[Mn(HCOO)_2]\cdot 1/3C_4H_8O_2$ and $[Mn(HCOO)_2]\cdot 1/3C_4H_8O$), studied earlier [10].

Properties of the bipy-contained inclusion compound with longer link are quite different. The "empty" matrix

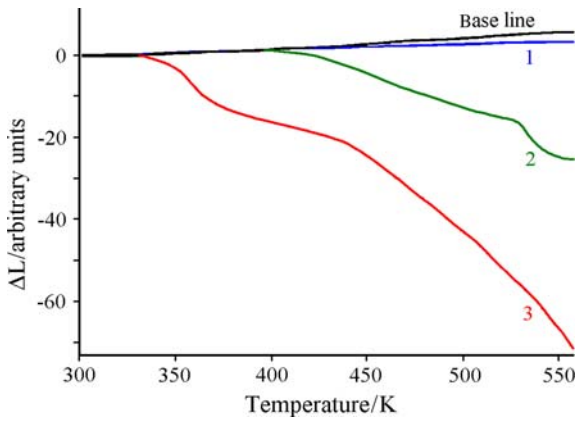

Fig. 9 Samples volume changing under heating, measured as the powder layer change (initial layer thickness 1 mm): *1* $[Zn_2(camph)_2dabco]\cdot DMF\cdot H_2O$, *2* $[Zn_2(camph)_2bipy]\cdot 3DMF\cdot H_2O$, *3* $[Zn_2(camph)_2bpe]\cdot 5DMF\cdot H_2O$

Table 4 Kinetic parameters of decomposition

Inclusion compound decomposition	"Model-free" E_a/kJ mol^{-1}	Decomposition steps/%	E_1 and E_2/kJ mol^{-1}	lg A
$[Zn_2(camph)_2dabco]$ DMF →	(variable)	21.7	89 ± 4	10.9 ± 0.7
$[Zn_2(camph)_2dabco]$ + DMF ↑	69 ± 3	78.3	63 ± 1	5.7 ± 0.2
$[Zn_2(camph)_2bipy]$ 3DMF →	(variable)	19.1	145 ± 1	17.5 ± 0.2
$[Zn_2(camph)_2bipy]$ + 3DMF ↑	99 ± 3	80.9	95 ± 4	9.0 ± 0.4
$[Zn_2(camph)_2bpe]$ 5DMF →	30 ± 3	27.2	28.1 ± 1.9	0.8 ± 0.08
$[Zn_2(camph)_2bpe]$ + 5DMF ↑	43 ± 2	72.8	47.7 ± 1.1	4.6 ± 0.1

structure (49% of the emptiness) is not achievable during heating. The matrix structure not only becomes deformed during DMF release, but fully collapses [2]. The activation energy value is, therefore, higher because for the endothermic decomposition reaction, the activation energy value will include both DMF elimination heat and matrix breakage (phase transfer) heat. The sample volume of $[Zn_2(camph)_2bipy]\cdot 3DMF\cdot H_2O$ decreases both during DMF moving off and after bipy removal (Fig. 9, curve 2).

The bpe-contained inclusion compound is destructed to roentgen-amorphous matrix substance, and does not restore the initial compound after interaction with DMF [2]. The "empty" matrix structure (more than half-empty one, with 55% of porous part) is not stable (thermodynamically and kinetically) at all, whereas the "filled" matrix structure can be synthesized only when it assembles during the synthesis: $\{Zn(NO_3)_2\cdot 6H_2O + H_2camph + DMF + bpe\}$, that is the expanded coordination compound matrix $[Zn_2(camph)_2bpe]\cdot 5DMF\cdot H_2O$ must be synthesized solely under the guest support, by assembling "around" DMF molecules [2]. Such structure must have low stability. Thermomechanical analysis shows that the "empty" structure of $[Zn_2(camph)_2bpe]$ with porous 55% volume is not stable at all (Fig. 9, curve 3); therefore, the sample volume decreases considerably and steadily during DMF removal and matrix structure collapse (330–500 K). Next sample volume decrease (520–560 K) is connected with bpe removal. The sharp increase of volume (at 560 K) can be connected with crystallization of new phases.

Conclusions

The decomposition of all inclusion compounds begins from dehydration process, although steps are not too much pronounced. We took away the mass loss from curves beginning (on the bases of DTG curves), so that the residuary mass loss (of DMF solely) stick to 10.0, 23.8 and 33.5% for dabco, bipy, bpe compounds, respectively. Curves onsets are partially distorted; the drastic decrease of activation energies on the very beginning of curves (Figs. 3, 5, 7) is connected with this context. These refined TG curves (Fig. 2 as example) are used for kinetic analysis. So calculated kinetic parameters include these accuracy errors and have limited precision. Nevertheless, their comparison is quite reasonable in this specific compound series with different host matrices and the same guest molecules: with lengthening linker ligands {4.5 (dabco), 8.0 (bipy) and 10.5 Å (bpe)} and with increasing free volumes in the frameworks (31, 49 and 55%).

Both the structure of the dabco-contained inclusion compound, and the "empty" matrix structure are rather rigid and stable because of the link shortness; this results in middle value of activation energy of the decomposition: for the elastic deformation (without destruction) of the matrix structure during DMF release.

The structure of the bipy-contained inclusion compound with longer link is not very stable. The "empty" matrix structure is not achievable during heating. The matrix structure not only becomes deformed during DMF release, but fully collapses; the activation energy value of decomposition is slightly higher than for the previous compound.

The bpe-contained inclusion compound is destructed during the decomposition and does not restore the initial compound after interaction with DMF. The "empty" matrix structure is not stable at all, whereas the "filled" matrix structure can be synthesized only when it assembles during the synthesis [2].

The enlargement of channels profiles (from dabco-compound to bipy-compound and to bpe-compound) decreases activation energy values, but the contribution of structure stability is essential too. It is worth to notice that two decomposition steps are relatively similar (19.1–27.2 and 72.3–80.9%) for three compounds, the activation energy has middle value for dabco-compound, maximal for bipy-compound and minimal for bpe-compound (in any calculation approach (Table 4). This correlates with structural changes of compounds under decomposition.

Similar properties are known for some more simple matrix: such "empty" host matrix as $[Zn(Py)_4(NO_3)_2]$ (where Py = pyridine) is thermodynamically unstable and does not exist at all (even in the system with liquid

pyridine); the appropriate inclusion compound $[Zn(Py)_4(NO_3)_2]\cdot 2Py$ exists, but decomposes in such manner: $[Zn(Py)_4(NO_3)_2]\cdot 2Py \rightarrow [Zn(Py)_3(NO_3)_2] + 3Py\uparrow$ [11, 12]. This phenomenon was named the contact stabilization of host complex molecules [13].

The large majority of recently published papers about thermal transformations of inclusion compounds cover the properties of clay intercalates [14–17]. The layered inclusion compounds have one peculiar behaviour, the high stability of the host matrix itself and the easy exchange of the guest molecules. The kinetic stability of inclusion compounds, based on the coordination compounds matrices, depends often on the host structure stability [10–13]. The clearing-up of the regularities between the host structure and the whole substance stability is important for the inclusion compounds chemistry.

Acknowledgements The authors are grateful to Netzsch Geraetebau GmbH for the possibility to work with computer program "NETZSCH Thermokinetics 2" and RFBR for the financial support (Grants 07-03-00436 and 07-03-91208).

References

1. Kitagawa S, Kitaura R, Noro S-I. Functional porous coordination polymers. Angew Chem Int Ed. 2004;43:2334–75.
2. Dybtsev DN, Yutkin MP, Peresypkina EV, Virovets AV, Serre Ch, Ferey G, et al. Isoreticular homochiral porous metal-organic structures with tunable pore size. Inorg Chem. 2007;46:6843–5.
3. Kissinger HE. Reaction kinetics in differential thermal analysis. Anal Chem. 1957;29:1702–6.
4. Friedman HL. Kinetics of thermal degradation of char-forming plastics from thermogravimetry. J Polym Sci C. 1963;6:183–95.
5. Ozawa T. A new method of analyzing thermogravimetric data. Bull Chem Soc Jpn. 1965;38:1881–6.
6. Ozawa T. Estimation of activation energy by isoconversion methods. Thermochim Acta. 1992;203(C):159–65.
7. Flynn JH, Wall LA. General treatment of the thermogravimetry of polymers. J Res Nat Bur Stand. 1966;70:478–523.
8. Opfermann J, Kaisersberger E. An advantageous variant of the Ozawa-Flynn-Wall analysis. Thermochim Acta. 1992;203(C): 167–75.
9. Opfermann JR, Kaisersberger E, Flammersheim HJ. Model-free analysis of thermo-analytical data-advantages and limitations. Thermochim Acta. 2002;391:119–27.
10. Logvinenko V, Dybtsev D, Fedin V, Drebushchak V, Yutkin M. The stability of inclusion compounds under heating. Part I. J Therm Anal Calorim. 2007;90:463–7.
11. Soldatov DV, Logvinenko VA, Dyadin YuA. The clathrates formation and phase equilibrium in the system Py-$Zn(NO_3)_2$. Zhurn Neorg Khimii. 1995;40:324–8 (in Russian).
12. Soldatov DV, Ukraintseva EA, Logvinenko VA, Dyadin YuA, Grachev EV, Manakov AYu. Thermodynamic dissociation constants for [MPy4(NO3)2]·2Py clathrates (M=Mn, Co, Ni, Cu). Supramol Chem. 2000;12:237–46.
13. Dyadin YuA, Soldatov DV, Logvinenko VA, Lipkowski J. Contact stabilization of host complex molecules during clathrate formation: the pyridine-zinc nitrate and the pyridine-cadmium nitrate systems. J Coord Chem. 1996;37:63–75.
14. Chow WS, Lok SK. Thermal properties of poly(lactic acid)/organo-montmorillonite nanocomposites. J Therm Anal Calorim. 2009;95:627–32.
15. Snircoval S, Jona E, Lajdova L, Jorik V, Drabik M, Pajtasova M, et al. Ni-exchanged montmorillonite with methyl-, dimethyl- and trimethylamine and their thermal properties. J Therm Anal Calorim. 2009;96:63–6.
16. Khan AH, Nurnabi M, Bala P. Studies on thermal transformation of Na–montmorillonite–glycine intercalation compounds. J Therm Anal Calorim. 2009;96:929–35.
17. Bakon KH, Palmer SJ, Frost RL. Thermal analysis of synthetic reevesite and cobalt substituted reevesite $(Ni,Co)_6Fe_2(OH)_{16}(CO_3)\cdot 4H_2O$. J Therm Anal Calorim. 2009. doi:10.1007/s10973-009-0145-x.